
Article:
Quirk, James A., Lazarov, Vlado K. orcid.org/0000-0002-4314-6865 and McKenna, Keith P. orcid.org/0000-0003-0975-3626 (2019) Electronic Properties of {112} and {110} Twin Boundaries in Anatase TiO2. Advanced Theory and Simulations. ISSN 2513-0390

https://doi.org/10.1002/adts.201900157

ADVANCED THEORY AND SIMULATIONS
www.advtheorysimul.com

Electronic Properties of {112} and {110} Twin Boundaries in Anatase TiO_2

James A. Quirk, Vlado K. Lazarov, and Keith P. McKenna*

First-principles calculations of the electronic structure and charge-trapping behavior of Σ3 {112} and Σ1 {110} twin boundaries (TBs) in anatase TiO_2 are performed using an accurate hybrid density functional theory approach. The former is characterized experimentally using transmission electron microscopy (TEM) and very good agreement on the structure is found. The {110} twin has not yet been observed but TEM and scanning tuneling microscopy (STM) image simulations are presented to aid experimental identification. Holes are found to trap in a polaronic configuration at both the twin boundaries. The {112} TB presents more favorable sites for hole polaron formation at the boundary with trapping energies 0.16–0.18eV, more favorable than the bulk. The {110} TB presents hole polaron trapping sites ranging from 0.07 eV, less favorable, to 0.14 eV, more favorable, than the bulk. Neither boundary is found to favor electron trapping, indicating they are relatively benign to the performance of anatase as an *n*-type conductor.

1. Introduction

The behavior of charge carriers in anatase TiO_2 is of utmost importance to its applications in energy generation as a photocatalyst,[1–3] as an *n*-type transport layer in solar cells,[4–6] and as a cathode in batteries.[7–9] Electrons or holes introduced by photoexcitation or charge injection can become trapped at point defects (vacancies or impurities), extended defects (such as grain boundaries, dislocations, or surfaces), or in the perfect lattice where the charge carrier introduces a lattice polarization (polaronic self-trapping).[10–15] The formation of small polarons in TiO_2 can affect the adsorption and reaction of molecules at surfaces[16] and lead to reduced conductivity and increase charge carrier recombination, which is detrimental to the performance of solar cells. It is known from extensive theoretical and experimental studies that holes can self-trap on oxygen ions (forming O^- species) in bulk anatase.[17,18] Large anatase single crystals are unstable so anatase is usually fabricated by sintering nanocrystals grown through a sol–gel process.[19,20] Polycrystalline systems such as these exhibit large numbers of extended defects which are expected to alter carrier mobility and polaron formation, but remain relatively poorly understood due to the difficulty of probing these structures experimentally. Approaches such as transmission electron microscopy (TEM) and scanning tunneling microscopy (STM) can provide some insight, but the complex nature of polycrystalline systems can make it challenging to confidently interpret images. First-principles predictions can provide insight at the atomic scale and narrow down possible interpretations of experimental results.

Here, we present first principles modeling of the atomic and electronic structure of the Σ3 {112} and Σ1 {110} twin boundaries (TBs) in anatase using accurate hybrid density functional theory (DFT) alongside simulated TEM and STM images to aid with comparison to experiment. Both TBs are found to have low formation energies and so are expected to occur frequently, a prediction supported by the experimental evidence of Σ3 {112} TBs in hydrothermally coarsened samples of anatase.[21–24] It is found that both TBs alter hole polaron trapping energies—with more favorable traps at the Σ3 {112} TB and less favorable traps at the Σ1 {110}—but neither provides sites for electron trapping nor are new states introduced in the band gap. For this reason, we predict that these TBs will be relatively benign to the electron mobility in anatase used an *n*-type electrode, but trapped holes if present (e.g., due to UV absorption) may lead to increased charge carrier recombination. Similarly, hole traps at interfaces in the bulk could pose problems for photocatalysis as it could prevent charge from being able to effectively migrate to surface sites and facilitate chemical reactions.

2. Results

2.1. Atomic Structure and Image Simulation

The most stable structures of the Σ3 {112} and Σ1 {110} TBs were identified using the systematic screening approach described in Setion 4. The Σ3 {112} and Σ1 {110} have formation energies, γ, of 0.30 Jm^{-2} and 0.34 Jm^{-2} and excess volumes, ΔV, of 0.02 Å and 0.06 Å, respectively. The optimized structures of each TB and simulated TEM images are shown in **Figure 1**. The Σ1 {110} TB

J. A. Quirk, Prof. V. K. Lazarov, Prof. K. P. McKenna
Department of Physics
University of York
Heslington, North Yorkshire YO10 5DD, UK
E-mail: jaq502@york.ac.uk

The ORCID identification number(s) for the author(s) of this article can be found under https://doi.org/10.1002/adts.201900157

DOI: 10.1002/adts.201900157

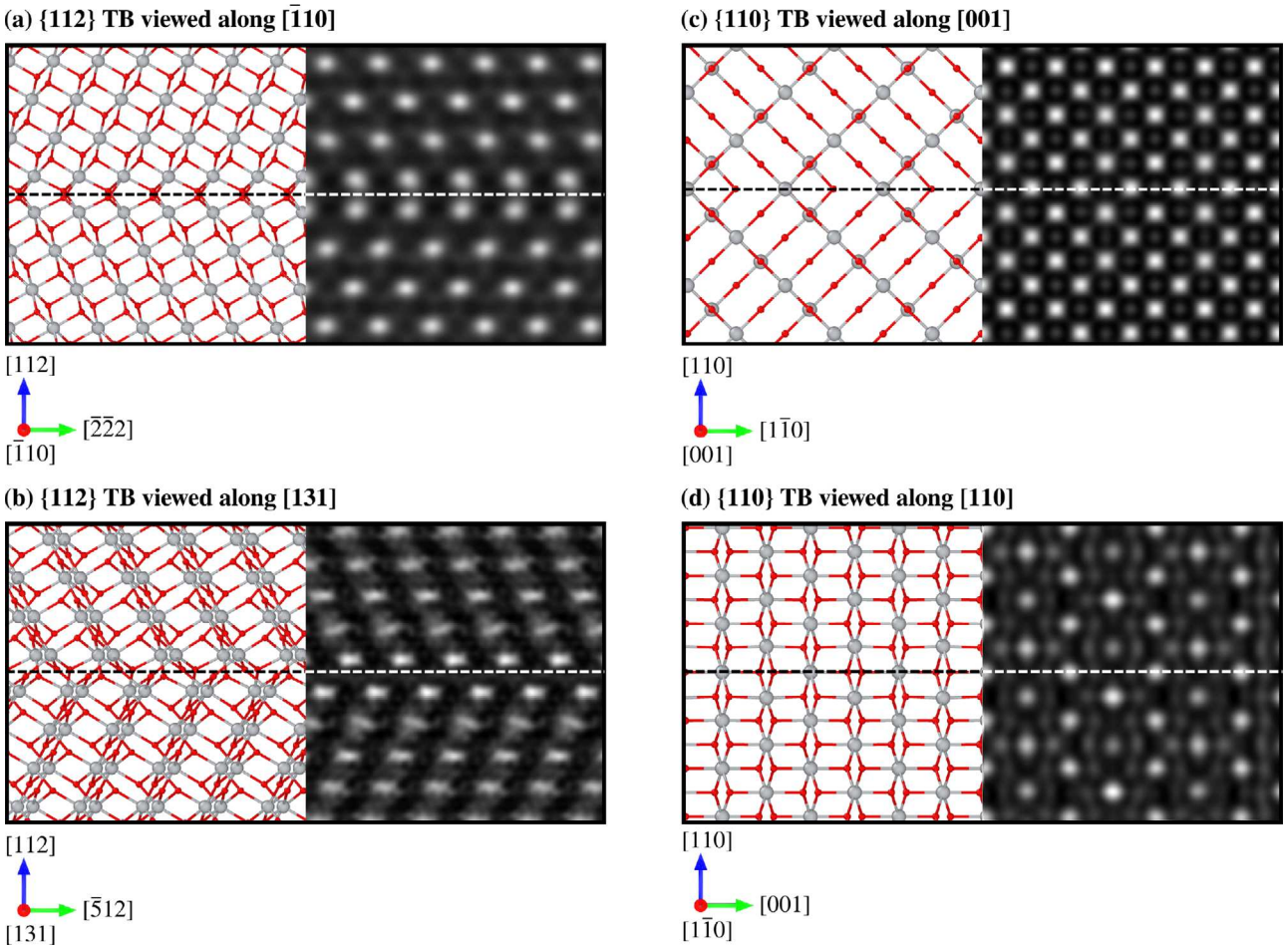

Figure 1. Structure and simulated TEM images for a) Σ3 {112} TB viewed along [110] (–12 nm defocus) and b) viewed along [131] (10 nm defocus). Structure and simulated TEM images c) Σ1 {110} TB viewed along [001] (2 nm defocus) and d) viewed along [110] (5 nm defocus). Note that the Σ1 {110} TB is invisible to TEM in these projections. Titanium and oxygen ions are represented by gray spheres and red spheres, respectively.

adopts a mirror symmetric configuration, whereas the Σ3 {112} TB has one grain translated by 2.68 Å in the [110] direction. Neither TB imposes significant strain on the lattice; the Σ1 {110} TB causes Ti-O bonds to be lengthened by about 1% and the Σ3 {112} TB shows no appreciable change in bond lengths. All atoms in both TBs are properly coordinated (i.e., 6-coordinated Ti and 3-coordinated O) with no dangling bonds. Previous theoretical work on anatase surfaces using the same functional has shown that the presence of undercoordinated Ti sites can allow electrons to self-trap in anatase. Therefore, it could be expected that neither TB is capable of trapping electrons. However, the {112} TB exhibits local bonding character similar to that of rutile and brookite,[22,23] which might intuitively suggest that its charge-trapping behavior is more like that of rutile (i.e., able to trap electrons but not trap holes[17,25,26]) than that of anatase. Comparatively, the bonding in the {110} TB is far closer to that of anatase and it might be expected that its trapping behavior would be similar to that of bulk anatase. However, as we show below, these naïve assumptions based on structure alone are not correct.

The Σ3 {112} TB has been experimentally observed in samples of hydrothermally coarsened anatase nanoparticles.[23] A simulated high-resolution TEM (HRTEM) image produced from the optimized structure of the Σ3 {112} TB viewed along [131] is in extremely good qualitative agreement with an experimental HRTEM image of a twinned anatase crystal viewed in the same projection (**Figure 2**). The Σ1 {110} TB is extremely high-symmetry and undergoes negligible relaxation during geometry optimization, this leads to difficulty in characterization with TEM as illustrated by the simulated images. The structure of the {110} TB can be better visualized as a change in the bonding direction of the characteristic "bridging" oxygens on the (001) surface of anatase, suggesting that surface-sensitive techniques could be better suited to detecting this boundary. We propose that STM would be sufficient to resolve a change of direction in bridging oxygens (**Figure 3**). It is possible to grow thin films of [001] oriented anatase on strontium titanate with a small lattice mismatch between both materials.[27] Given that the Σ1{110} boundary involves a 90° rotation about the [001] axis with relatively low strain, we predict that this boundary could occur in epitaxially grown thin films that are constrained to the cubic geometry of the strontium titanate substrate. Such samples would be suitable for imaging using STM.

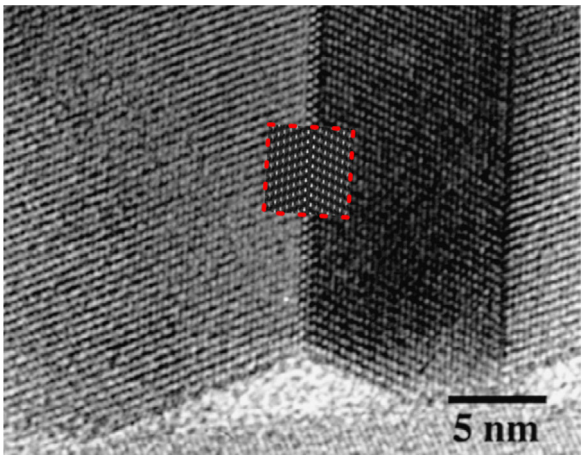

Figure 2. HRTEM image of a twinned anatase nanoparticle, viewed down {131}. Reproduced with permission.[23] Copyright 1999, Mineralogical Society of America. The inlaid image (red dashed border) is a simulated HRTEM image, demonstrating close agreement with experiment.

2.2. Electronic Structure and Trapping

For each TB, we calculate the projected density of states (PDOS) for atoms in the vicinity of the TB, as well as for the bulk-like region of the grain far from the TB plane (**Figure 4**). With respect to holes, the Σ3 {112} has more states near the valence band maximum (VBM) in the TB region than in the bulk region which indicates hole trapping behavior. Conversely, the Σ1 {110} shows that some states move away from the VBM indicating less favorable hole trapping. Both PDOS show that states move down to near the conduction band minimum (CBM) at the TB, which is indicative of electron trapping behavior. Neither TB alters the band gap or introduces any gap states, which indicates that neither boundary introduces trap states in its equilibrium geometry. To support predictions from the PDOS we produce charge density isosurfaces for electrons and holes added vertically to the TB (i.e., without any geometry optimization in order to visualize the character of the band edges). In the Σ3 {112}, the charge density isosurface for a vertically added hole shows a strong preference toward O sites in the vicinity of the TB, which is consistent with predictions based on the PDOS. For a vertically added hole in the Σ1 {110}, we see that the density isosurface avoids O sites directly ion the TB plane as expected from the PDOS. There is, however, a small preference toward O sites directly adjacent to the TB, which will correspond to states that are just below the VBM. With regard to electrons, we find that a vertically added electron in the Σ1 {110} shows a strong preference toward Ti sites in the TB plane as suggested by the PDOS. However, in the Σ3 {112} the density isosurface shows no appreciable preference toward any Ti site, contrary to the PDOS. This can be explained by the fact that the movement of states downward is not as pronounced in the Σ3 {112} as it is in the Σ1 {110}.

The above results indicate that these TBs do not significantly perturb the electronic structure of bulk anatase. To assess their impact on polaronic trapping, we calculated polaron trapping energies for all symmetrically inequivalent sites in the TB region of each supercell. It was found that neither TB allows the formation of small electron polarons in anatase, which is in agreement

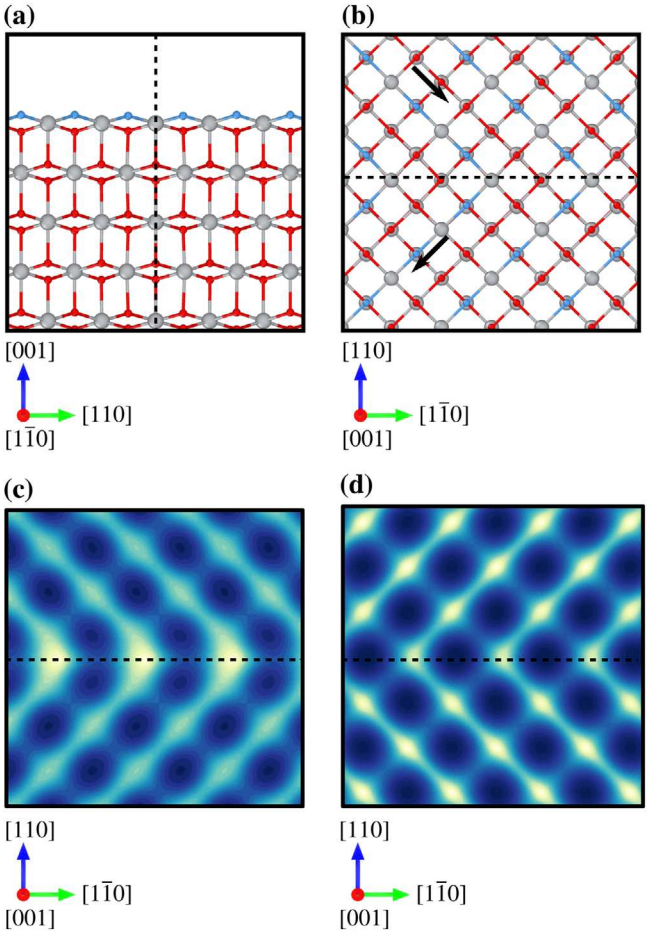

Figure 3. a) An unreconstructed (001) surface with a Σ1 {110} TB, viewed along [1$\bar{1}$0] b) an unreconstructed (001) surface containing a {110} TB viewed along [001] together with simulated STM images for c) filled states and d) empty states. Dashed lines indicate the position of the TB. Titanium and oxygen ions are represented by gray spheres and red spheres, respectively. Characteristic bridging oxygen ions across the surface have been highlighted as blue spheres. Note how the direction of the bonding of the bridging oxygen ions (indicated by arrows) changes direction as the TB is crossed whereas in pristine anatase, the direction of the bridging bonds remains unchanged.

with previous theoretical work[25] and experimental evidence indicating that anatase has very high electron mobility.[28,29] Electron trap states at the TB indicated by the PDOS are more likely to be large, diffuse solutions akin to those seen in STM experiments on Nb-doped anatase.[17] Hole polarons could be successfully trapped at both sites in the Σ1 {110} and two out of three sites in the Σ3 {112} (**Figure 5**), with the third site not leading to a delocalized solution but leading to a polaron forming on the nearest TB O. The most stable hole polaron in the Σ {112} TB is shown in Figure 5a, which is 0.178 eV more stable than a bulk-like hole polaron. The most stable hole polaron in the Σ1 {110} TB is shown in Figure 5d, which is 0.147 eV more stable than a bulk-like hole polaron.

In spite of the fact that the Σ3 {112} TB exhibits rutile-like and brookite-like bonding, it does not mimic either phase with respect to polaron formation. Small electron polarons form in

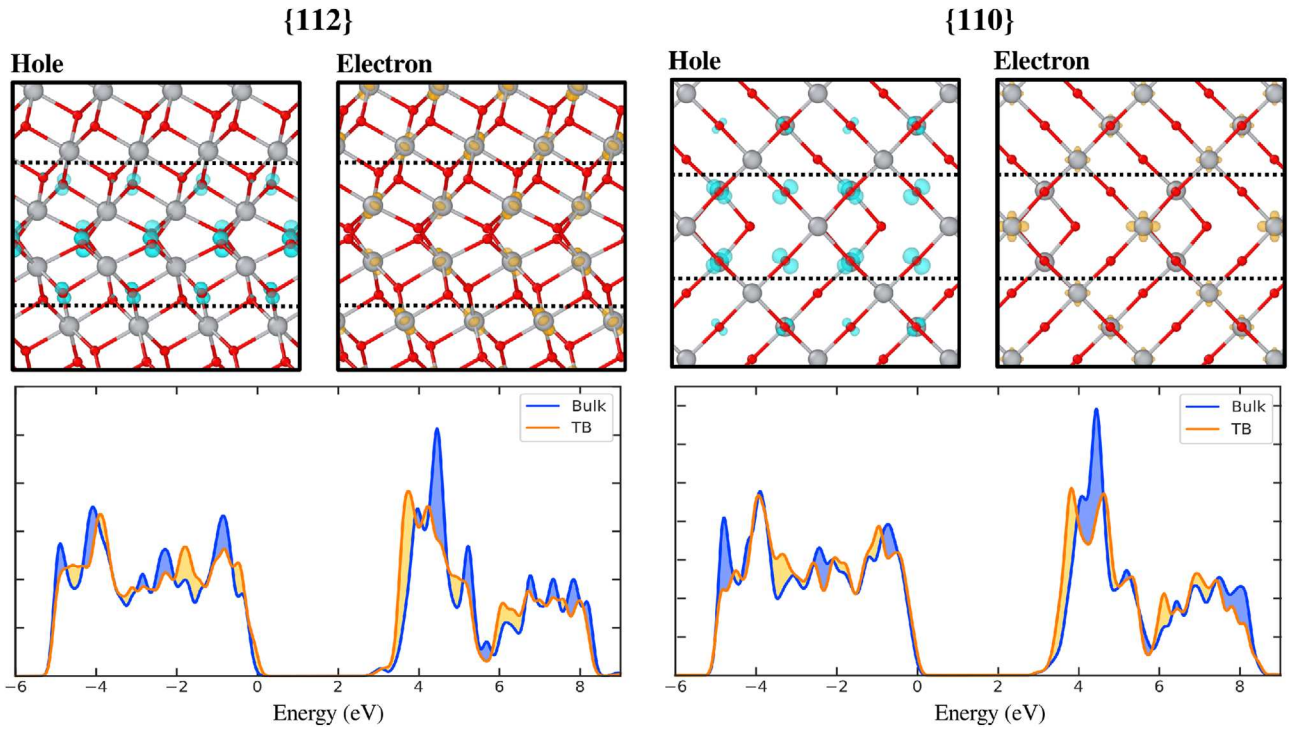

Figure 4. Charge density isosurfaces for vertically added electrons and holes (top) where the area bounded by dashed lines indicates the "TB region" (isosurface value is 0.005 a_0^{-3}). Also shown is the PDOS for a charge-neutral system, projected across the bulk-like region (blue) and the TB region (orange) of the {112} (left) and {110} (right) supercells. Shaded areas on the PDOS indicate where a region has a greater number of states of a given energy. Titanium and oxygen ions are represented by gray spheres and red spheres, respectively.

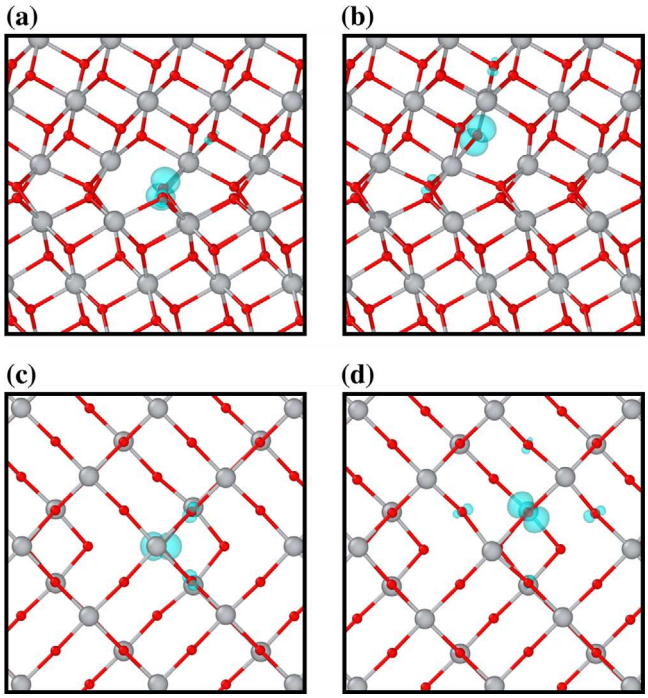

Figure 5. Hole polarons trapped at a) an O on the Σ3 {112} TB, b) an O adjacent to the Σ3 {112} TB, c) an O on the Σ1 {110} TB and, d) an O directly adjacent to the Σ1 {110} TB. The isosurface value is 0.01 a_0^{-3}. Titanium and oxygen ions are represented by gray spheres and red spheres, respectively.

rutile which are not present at the TB. In bulk brookite, there are two inequivalent O sites, both of which trap holes, but the relative trapping energies are not consistent with what we find for the TB; the brookite O with the higher polaron trapping energy corresponds to the Σ3 {112} with lower trapping energy, and vice versa.[25] The Σ1 {110} TB provides a far more favorable site directly adjacent to the boundary, while the site on the boundary is slightly less favorable. To provide further insight into the driving force for polaron site preference we analyzed strain and electrostatic contributions but could find no clear correlation (see Supporting Information). We note that the TBs considered here exhibit no undercoordination and differences in trapping energies are small. This is quite different to the situation in more general extended defects such as surfaces and grain boundaries where correlations between polaron stability and these quantities have been found previously.[12,30] In such a case, much more subtle effects may dictate the stability of polarons and identifying a simple predictive measure of polaron site preference is no longer straightforward.

The polarons modeled in these TBs lead to the presence of a defect level state in the band gap. The defect level of the most stable polaron trapped at each TB is significantly higher than the defect level of a bulk-like polaron (**Figure 6**). We propose that these differences would be possible to probe experimentally using photoluminescence (PL) spectroscopy, where a hole produced by photoabsorption could become self-trapped in the lattice.[31,32] As both TBs present more stable hole polarons than bulk anatase, the expectation is that there would be a higher concentration of polarons at the TB, which could be measured with spatially

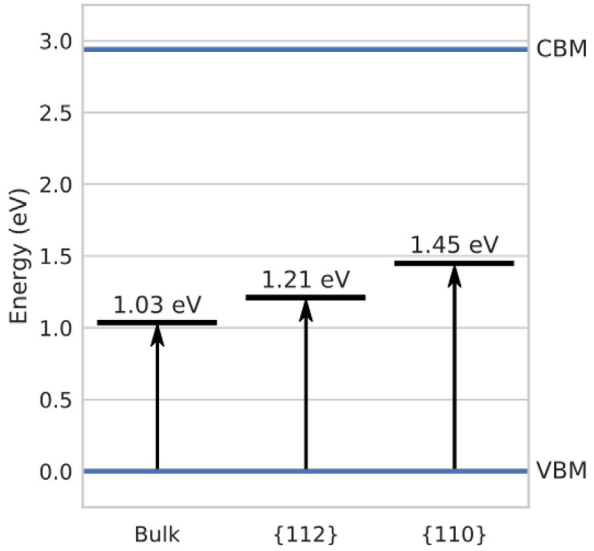

Figure 6. Defect levels of the most stable hole polarons in the bulk-like region, as well as the vicinity of the {112} and {110} TBs in anatase TiO_2. The VBM and CBM are marked as blue lines.

resolved PL. Furthermore, the defect levels of the TB polarons are higher in energy which would lead to photons emitted by recombination being red-shifted relative to recombination at a bulk-like polaron. The TBs considered in this work are modeled as they would occur in the bulk of the crystal, but it is also possible to probe polaron states at the surface using a scanning probe method such as STM.[17] If a sample of anatase could be produced where a TB terminates at the surface of a film, then a scanning probe method could also be utilized. It should be noted, however, that these polarons near the surface would have modified properties compared to those we have considered.

3. Conclusions

The atomic and electronic structure of two TBs in anatase (Σ3 {112} and Σ1 {110}) are investigated using a hydrid DFT approach. It was found that the optimized structure of the Σ3 {112} TB was in good agreement with experimental results based on a similarities between the simulated and real TEM images.[23] The predicted structure of the Σ1 {110} TB has very high symmetry, meaning that it would be extremely difficult to observe using methods such as electron microscopy. We propose scanning probe microscopy on (001) oriented anatase (e.g., as grown on $SrTiO_3$ (001)) could resolve this defect, and we provide simulated STM images to aid interpretation of experimental images.

Neither TB exhibits the formation of electron polarons, nor do any states form in the band gap. Due to this, we predict that neither defect would be significantly problematic when considering anatase as an *n*-type conductor aside from the increased possibility of recombination due to the higher concentration of trapped holes at the boundary. With regard to photocatalysis, it has been shown in previous studies that holes trapped at anatase surfaces can engage in water-splitting reactions.[16] If holes generated by incident light do not recombine with electrons, they may then become trapped at TB sites far from the surface of the crystal. This will lead to lower number of holes available at the surface to interact with adsorbates, thereby lowering the overall reaction rate. Additionally, it must be remembered that both TBs considered in this work are ideal cases with extremely high symmetry, and no dangling bonds or undercoordinated species. The polycrystalline anatase commonly found in devices could have point defects in the vicinity of the TBs, or could have lower symmetry extended defects that might prove to be much more harmful with respect to charge transport. This investigation has provided insight into the formation of polarons in anatase, but more work will be required to fully identify—and learn to counter—more malignant defects that could occur.

4. Computational Methods

All electronic structure calculations were carried out using hybrid-DFT, where a fraction Hartree–Fock (HF) exact exchange is mixed into the Perdew–Burke–Ernzerhof (PBE) functional[33] in order to correct the self-interaction error present in standard semilocal approximations for exchange–correlation.[34–36] We use the implementation of hybrid DFT within CP2K,[37] which employs two methods to reduce the computational cost of the HF part of the calculation. First, we use a truncated HF exchange functional (known as PBE0-TC-LRC[38,39]) in which, beyond a cutoff radius, PBE exchange is used instead of HF exchange. It is found that a cutoff radius of 6 Å is well converged with regard to lattice parameter and band gap. The second approach to reducing computational cost is the auxiliary density matrix method[40] in which exchange integrals are approximated through mapping onto smaller, more localized basis sets. For both titanium and oxygen, we use triple-ζ basis sets optimized from molecular calculations (MOLOPT)[41] and Goedecker–Teter–Hutter pseudopotentials available within CP2K. We use five multigrids with a relative cutoff of 60 Ry and the finest grid having a cutoff of 600 Ry. All geometry optimization is performed until the forces on ions are less than 0.01 eVÅ^{-1}. As CP2K only samples the Γ-point, a large supercell must be used to ensure sufficient effective *k*-point sampling in reciprocal space. A 5×5×2 supercell of bulk anatase containing 600 atoms is sufficient to yield lattice parameters of $a = b = 3.78$ Å and $c = 9.61$ Å which are within 1% of experimentally determined parameters. We employ 10.5% HF exchange, a fraction which ensures that the generalized Koopman's condition is obeyed to within 0.05 eV in bulk anatase.[25,42] This so-called Koopman's compliant functional is found to be in good agreement with experiment with regard to polaron formation.[25,43] A detailed description of the parameterization of this functional for anatase, and other TiO_2 polymorphs, is found in our previous work.

Our TBs are modeled in a periodic supercell containing two symmetrically equivalent boundaries. The dimensions of the supercells for the Σ3 {112} and Σ1 {110} were 16.1 × 16.4 × 37.4 Å and 21.5 × 19.2 × 27.1 Å, respectively. In such a cell the formation energy, γ, can be defined as

$$\gamma = \frac{E_{\mathrm{TB}} - NE_{\mathrm{Bulk}}}{2A} \quad (1)$$

where E_{TB} is the total energy of the optimized cell containing the TB, N is the number of formula units of anatase in the TB supercell, E_{Bulk} is the total energy of bulk anatase per formula unit, and A is the cross-sectional area of the TB supercell. During geometry optimization, only the supercell vector normal to the TB is allowed to relax, while the supercell vectors parallel to the TB are held fixed. We consider all possible rigid-body translations parallel to the TB plane in 0.5 Å steps. We also define the excess volume per unit of cross-sectional area caused by the TB, ΔV, as

$$\Delta V = \frac{V_{TB} - NV_{Bulk}}{2A} \tag{2}$$

where $V_{TB}^{Relaxed}$ is the volume of the optimized TB supercell and V_{Bulk} is the volume per formula unit of bulk anatase.

In order to test for the possibility of polaron formation on a given site, nearest neighbour ions are displaced 0.1 Å away to create a precursor potential well for trapping. The structure is then self-consistently optimized with an additional electron or hole present. If the charge remains localized, a small polaron configuration has been identified. We can then define a relative trapping energy, ΔE, as

$$\Delta E = E_{TB}^{Polaron} - E_{Bulk}^{Polaron} \tag{3}$$

where $E_{TB}^{Polaron}$ and $E_{Bulk}^{Polaron}$ are the total energies of a polaron trapped at a TB site and a bulk-like site, respectively.

Simulated HRTEM images were carried out on the optimized structures using the multislice method as implemented in QSTEM.[44,45] An accelerating potential of 200 kV and a spherical aberration of 0.05 mm was used in these simulations and defocus was applied to improve contrast in the images. The level of defocus present in an image is specified in the corresponding captions. Simple simulated STM images were produced using the Tersoff–Hamann approximation[46]; filled and empty states were probed using a bias energy of −2.5 eV and 5.0 eV, respectively.

Supporting Information

Supporting Information is available from the Wiley Online Library or from the author.

Acknowledgements

K.P.M. and V.K.L. acknowledge support from EPSRC (EP/P006051/1). This work made use of the facilities of Archer, the United Kingdom's national high-performance computing service, via our membership in the UK HPC Materials Chemistry Consortium, which is funded by EPSRC (EP/L000202/1). This project also made use of the Viking Cluster, which is a high-performance computation facility provided by the University of York. The authors are grateful for computational support from the University of York High Performance Computing service,Viking and the Research Computing team. All data created during this research are available by request from the University of York Research database at: https://doi.org/10.15124/dc471795-666c-4759-bd85-6b7ecce0925d.

Conflict of Interest

The authors declare no conflict of interest.

Keywords

density functional theory, polarons, titanium dioxide, twin boundaries

Received: August 13, 2019
Revised: September 25, 2019
Published online:

[1] A. Fujishima, K. Honda, *Nature* **1972**, *238*, 37.
[2] S. G. Kumar, L. G. Devi, *J. Phys. Chem. A* **2011**, *115*, 13211.
[3] D. Friedmann, C. Mendive, D. Bahnemann, *Appl. Catal. B-Environ.* **2010**, *99*, 398.
[4] Y. Bai, I. Mora-Sero, F. De Angelis, J. Bisquert, P. Wang, *Chem. Rev.* **2014**, *114*, 10095.
[5] H.-S. Kim, J.-W. Lee, N. Yantara, P. P. Boix, S. A. Kulkarni, S. Mhaisalkar, M. Grätzel, N.-G. Park, *Nano Lett.* **2013**, *13*, 2412.
[6] B. O'regan, M. Grätzel, *Nature* **1991**, *353*, 737.
[7] J. S. Chen, Y. L. Tan, C. M. Li, Y. L. Cheah, D. Luan, S. Madhavi, F. Y. C. Boey, L. A. Archer, X. W. Lou, *J. Am. Chem. Soc.* **2010**, *132*, 6124.
[8] Y.-G. Guo, Y.-S. Hu, W. Sigle, J. Maier, *Adv. Mater.* **2007**, *19*, 2087.
[9] G. F. Ortiz, I. Hanzu, T. Djenizian, P. Lavela, J. L. Tirado, P. Knauth, *Chem. Mater.* **2008**, *21*, 63.
[10] P. Deák, B. Aradi, T. Frauenheim, *Phys. Rev. B* **2012**, *86*, 195206.
[11] B. J. Morgan, G. W. Watson, *Surf. Sci.* **2007**, *601*, 5034.
[12] S. K. Wallace, K. P. Mckenna, *J. Phys. Chem. C* **2015**, *119*, 1913.
[13] T. Wosiński, *J. Appl. Phys.* **1989**, *65*, 1566.
[14] E. Maras, M. Saito, K. Inoue, H. Jønsson, Y. Ikuhara, K. P. McKenna, *Acta Mater.* **2019**, *163*, 199.
[15] A. Stoneham, J. Gavartin, A. Shluger, A. Kimmel, D. M. Ramo, H. Rønnow, G. Aeppli, C. Renner, *J. Phys-Condens. Mat.* **2007**, *19*, 255208.
[16] C. Di Valentin, *J. Phys-Condens. Mat.* **2016**, *28*, 074002.
[17] M. Setvin, C. Franchini, X. Hao, M. Schmid, A. Janotti, M. Kaltak, C. G. Van de Walle, G. Kresse, U. Diebold, *Phys. Rev. Lett.* **2014**, *113*, 086402.
[18] T. Berger, M. Sterrer, O. Diwald, E. Knözinger, D. Panayotov, T. L. Thompson, J. T. Yates, *J. Phys. Chem. B* **2005**, *109*, 6061.
[19] A. A. Gribb, J. F. Banfield, *Am. Miner.* **1997**, *82*, 717.
[20] M. Grätzel, *J. Sol-Gel Sci. Techn.* **2001**, *22*, 7.
[21] R. L. Penn, J. F. Banfield, *Geochim. Cosmochim. Ac.* **1999**, *63*, 1549.
[22] R. L. Penn, J. F. Banfield, *Am. Mineral.* **1998**, *83*, 1077.
[23] R. L. Penn, J. F. Banfield, *Am. Mineral.* **1999**, *84*, 871.
[24] P. I. Gouma, M. J. Mills, *J. Am. Ceram. Soc.* **2001**, *84*, 619.
[25] A. R. Elmaslmane, M. B. Watkins, K. P. McKenna, *J. Chem. Theory Comput.* **2018**, *14*, 3740.
[26] S. Yang, A. Brant, N. Giles, L. Halliburton, *Phys. Rev. B* **2013**, *87*, 125201.
[27] H. Seo, A. B. Posadas, C. Mitra, A. V. Kvit, J. Ramdani, A. A. Demkov, *Phys. Rev. B* **2012**, *86*, 075301.
[28] B. Sun, A. V. Vorontsov, P. G. Smirniotis, *Langmuir* **2003**, *19*, 3151.
[29] L. Forro, O. Chauvet, D. Emin, L. Zuppiroli, H. Berger, F. Levy, *J. Appl. Phys.* **1994**, *75*, 633.
[30] M. J. Wolf, K. P. McKenna, A. L. Shluger, *J. Phys. Chem. C* **2012**, *116*, 25888.
[31] K. Wakabayashi, Y. Yamaguchi, T. Sekiya, S. Kurita, *J. Lumin.* **2005**, *112*, 50.
[32] C. C. Mercado, F. J. Knorr, J. L. McHale, *ACS Nano* **2012**, *6*, 7270.
[33] J. P. Perdew, K. Burke, M. Ernzerhof, *Phys. Rev. Lett.* **1996**, *77*, 3865.

[34] J. P. Perdew, R. G. Parr, M. Levy, J. L. Balduz Jr, *Phys. Rev. Lett.* **1982**, *49*, 1691.
[35] M. Levy, J. P. Perdew, V. Sahni, *Phys. Rev. A* **1984**, *30*, 2745.
[36] J. P. Perdew, M. Levy, *Phys. Rev. B* **1997**, *56*, 16021.
[37] J. VandeVondele, M. Krack, F. Mohamed, M. Parrinello, T. Chassaing, J. Hutter, *Comput. Phys. Commun.* **2005**, *167*, 103.
[38] M. Guidon, J. Hutter, J. VandeVondele, *J. Chem. Theory Comput.* **2009**, *5*, 3010.
[39] J. Spencer, A. Alavi, *Phys. Rev. B* **2008**, *77*, 193110.
[40] M. Guidon, J. Hutter, J. VandeVondele, *J. Chem. Theory Comput.* **2010**, *6*, 2348.
[41] J. VandeVondele, J. Hutter, *J. Chem. Phys.* **2007**, *127*, 114105.
[42] J. J. Carey, K. P. McKenna, *J. Phys. Chem. C* **2018**, *122*, 27540.
[43] A. Elmaslmane, J. Wetherell, M. Hodgson, K. McKenna, R. Godby, *Phys. Rev. Mater.* **2018**, *2*, 040801.
[44] C. T. Koch, *PhD Thesis*, Arizona State University, **2002**.
[45] J. M. Cowley, A. F. Moodie, *Acta Crystallogr.* **1957**, *10*, 609.
[46] J. Tersoff, D. Hamann, *Phys. Rev. B* **1985**, *31*, 805.